Energy, water, and carbon fluxes in a loblolly pine stand: Results from uniform and gappy canopy models with comparisons to eddy flux data

Conghe Song,[1] Gabriel Katul,[2] Ram Oren,[2] Lawrence E. Band,[1] Christina L. Tague,[3] Paul C. Stoy,[2,4] and Heather R. McCarthy[5]

Received 9 February 2009; revised 27 July 2009; accepted 2 September 2009; published 16 December 2009.

[1] This study investigates the impacts of canopy structure specification on modeling net radiation (R_n), latent heat flux (LE) and net photosynthesis (A_n) by coupling two contrasting radiation transfer models with a two-leaf photosynthesis model for a maturing loblolly pine stand near Durham, North Carolina, USA. The first radiation transfer model is based on a uniform canopy representation (UCR) that assumes leaves are randomly distributed within the canopy, and the second radiation transfer model is based on a gappy canopy representation (GCR) in which leaves are clumped into individual crowns, thereby forming gaps between the crowns. To isolate the effects of canopy structure on model results, we used identical model parameters taken from the literature for both models. Canopy structure has great impact on energy distribution between the canopy and the forest floor. Comparing the model results, UCR produced lower R_n, higher LE and higher A_n than GCR. UCR intercepted more shortwave radiation inside the canopy, thus producing less radiation absorption on the forest floor and in turn lower R_n. There is a higher degree of nonlinearity between A_n estimated by UCR and by GCR than for LE. Most of the difference for LE and A_n between UCR and GCR occurred around noon, when gaps between crowns can be seen from the direction of the incident sunbeam. Comparing with eddy-covariance measurements in the same loblolly pine stand from May to September 2001, based on several measures GCR provided more accurate estimates for R_n, LE and A_n than UCR. The improvements when using GCR were much clearer when comparing the daytime trend of LE and A_n for the growing season. Sensitivity analysis showed that UCR produces higher LE and A_n estimates than GCR for canopy cover ranging from 0.2 to 0.8. There is a high degree of nonlinearity in the relationship between UCR estimates for A_n and those of GCR, particularly when canopy cover is low, and suggests that simple scaling of UCR parameters cannot compensate for differences between the two models. LE from UCR and GCR is also nonlinearly related when canopy cover is low, but the nonlinearity quickly disappears as canopy cover increases, such that LE from UCR and GCR are linearly related and the relationship becomes stronger as canopy cover increases. These results suggest the uniform canopy assumption can lead to underestimation of R_n, and overestimation of LE and A_n. Given the potential in mapping regional scale forest canopy structure with high spatial resolution optical and Lidar remote sensing plotforms, it is possible to use GCR for up-scaling ecosystem processes from flux tower measurements to heterogeneous landscapes, provided the heterogeneity is not too extreme to modify the flow dynamics.

Citation: Song, C., G. Katul, R. Oren, L. E. Band, C. L. Tague, P. C. Stoy, and H. R. McCarthy (2009), Energy, water, and carbon fluxes in a loblolly pine stand: Results from uniform and gappy canopy models with comparisons to eddy flux data, *J. Geophys. Res.*, *114*, G04021, doi:10.1029/2009JG000951.

[1]Department of Geography, University of North Carolina at Chapel Hill, Chapel Hill, North Carolina, USA.
[2]Nicholas School of Environment, Duke University, Durham, North Carolina, USA.
[3]Donald Bren School of Environment and Management, University of California, Santa Barbara, California, USA.
[4]School of GeoSciences, University of Edinburgh, Edinburgh, UK.
[5]Department of Earth System Science, University of California, Irvine, California, USA.

0148-0227/09/2009JG000951

1. Introduction

[2] Forest canopies regulate exchanges of energy, water and carbon with the atmosphere, particularly via leaf stomata, the primary corridors for transpiration and carbon assimilation [*Betts et al.*, 1997; *Pukkala et al.*, 1991; *Sellers et al.*, 1997; *Tang et al.*, 1999; *McGuire et al.*, 2001; *Ryan*, 2002; *Gedney et al.*, 2006; *Betts et al.*, 2007]. Among the key drivers of stomatal regulation, the light environment is

highly influential because of (1) the strong vertical heterogeneity imposed by the leaf transmission and interception, and (2) the nonlinear response of both leaf stomata and photosynthesis to light. Within tall canopies, photosynthetically active radiation (PAR) can vary by a factor of five or more while concomitant vertical changes in, for example, meteorological drivers such as vapor pressure deficit may be on the order of 20% or less [*Sinclair et al.*, 1976; *Ewers and Oren*, 2000; *Lai et al.*, 2000]. Understanding the sensitivity of energy, water and carbon fluxes to the representation of canopy structure in ecosystem models is essential in scaling up fluxes from canopies to landscapes.

[3] Detailed three-dimensional or multilayer radiation transfer models have been developed (see, for example, reviews by *Goel* [1988], *Myneni et al.* [1989], *Wang and Jarvis* [1990], and *Chen et al.* [2000]), but they are often too computationally expensive and "over-parameterized" with respect to the available input, especially when addressing large-scale ecological questions on annual or interannual time scales. Attempts to represent the canopy over large spatial domains and long-temporal integrations often adopt a simpler approach, and assume that the canopy can be represented by a uniform isotropic turbid medium, as employed by a number of models: FOREST-BGC [*Running and Coughlan*, 1988], Hybrid [*Friend et al.*, 1997], 3-PG [*Landsberg and Waring*, 1997], SDGVM [*Woodward et al.*, 1998] and RHESSys [*Tague and Band*, 2004]. However, even uniform crop canopies rarely meet the isotropic turbid medium assumption [*Suits*, 1983], and leaves in forest canopies are usually clumped at multiple spatial scales, severely violating the homogeneity assumption [*Chen and Leblanc*, 1997; *Ni et al.*, 1997; *Kucharik et al.*, 1999; *Yang et al.*, 2001]. Understanding these compromises in terms of model skill that are accrued by making such assumptions is a logical first step for developing process-based ecosystem models that are robust in long-term space-time integration.

[4] Recently, *Song and Band* [2004] developed a computationally efficient model for the mean and variation of PAR (MVP) under forest canopies. MVP accounts for the role of gaps in light propagation through forest canopies based on the geometric-optical theory [*Li et al.*, 1995], and it was tested with observed radiation data from the Southern Study Area–Old Black Spruce (SSA-OBS) stand of the BOREAS project [*Sellers et al.*, 1997]. Our objective is to extend this work and quantify differences in estimates of energy, water and carbon fluxes obtained using a moderately complex but more realistic representation of canopy structure relative to those obtained using the more commonly used uniform canopy representation. We perform this comparison for a temperate forest ecosystem by coupling the state-of-the-art evapotranspiration and photosynthesis models with two contrasting canopy representations for radiation interception: a uniform canopy representation (UCR) that uses Beer's law and a gappy canopy representation (GCR) that uses an improved version of MVP. The differences between the two canopy representations with identical model parameters are evaluated and compared with measurements of flux data at the site. We further performed a series of sensitivity analyses of both approaches over a broader range of canopy structure parameters in order to generalize our understanding of the relative importance of canopy s re representations in terrestrial ecosystem models. It is envisaged that a broader impact of this work will be to guide future efforts to parsimoniously scale-up fluxes from canopies to landscape.

2. Study Site and Data

[5] The study site is an even-aged loblolly pine (*Pinus taeda*) stand planted in 1984, located in the Blackwood Division of Duke Forest, near Durham, North Carolina (35° 58′ 41.4″ N, 79° 5′ 39.1″ W). Due to natural regeneration, the stand now has two distinct canopy layers, a dominant upper layer of loblolly pine and a subdominant layer of hardwoods. Mean annual precipitation at the site is 1140 mm, and mean annual temperature is 15.5°C. Soils are acidic Hapludalf, with a clayey loam in the upper 0.3 m, and a clay pan below, minimizing drainage [*Oren et al.*, 1998]. The local topographic variations are sufficiently small (<5% slopes) such that their impact on micrometeorological flux measurements can be neglected.

[6] Eddy-covariance measurements (ECMs) of turbulent heat, water and CO_2 fluxes, along with ancillary micrometeorological measurements, have been conducted at the research forest since 1998 as part of the AmeriFlux network and the FLUXNET project [*Baldocchi et al.*, 2001]. The meteorological tower is situated in plot 1, a control plot of the Free Air CO_2 Enrichment (FACE) experiment [*Schäfer et al.*, 2002]. The semianalytical flux footprint model of *Hsieh et al.* [2000] extended to two dimensions by *Detto et al.* [2006] was used to ensure that ECMs were not contaminated by elevated CO_2 rings in other areas of the same pine forest [*Stoy et al.*, 2006]. Model evaluation was based on ECMs collected during May to September 2001.

[7] The modeled evapotranspiration and photosynthesis are driven by measured half hourly incident solar radiation, precipitation, air temperature (T_a), relative humidity (H_r), mean wind speed (u), and volumetric soil water content (θ_v) and soil temperature (T_s), all of which are averaged (or aggregated) every 30 min. Six Parameters were used to characterize the canopy structure. These parameters include upper and lower canopy boundary heights, stem density, average horizontal crown radius, crown shape, and leaf area index. For the simpler model, only LAI was used. All canopy structural parameters were obtained based on the annual stand inventory combined with allometric relationships measured in the field [*Song*, 2007]. Temporal dynamics of LAI were reconstructed using data on leaf litterfall mass and timing, specific leaf area, leaf elongation rates, and fascicle, flush and branch counts [*McCarthy et al.*, 2007]. Figure 1 shows the temporal dynamics of LAI from May to September 2001. Throughout the paper, we refer to *canopy* as the space above the ground where leaves are distributed, and *stand* as the entity that includes both canopy and the forest floor. We did not explicitly include understory brush and herbaceous vegetation in the model as their distribution is limited.

3. Model Description

3.1. Modeling Radiation Interception by Forest Canopies

[8] For UCR, Beer's law, as described by *Campbell and Norman* [1998], was used to model canopy radiation

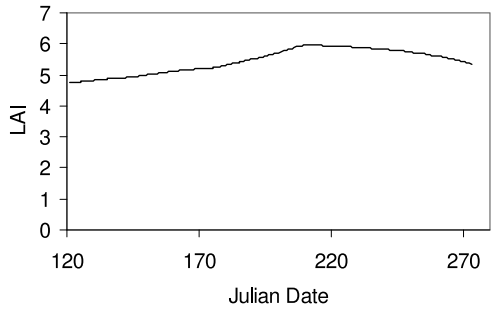

Figure 1. Temporal trajectory of LAI for the loblolly pine stand from May to September 2001. Details of LAI reconstruction are given by *McCarthy et al.* [2007].

interception (see Appendix A for details). Simulation of canopy radiation interception for the GCR is based on MVP, as described by *Song and Band* [2004]. MVP was originally developed for PAR transmission for a single species canopy. Here, it is modified to account for a mixed species canopy and applied to simulate the propagation of PAR, near infrared radiation (NIR) and long wave radiation separately. The total absorbed shortwave radiation is the sum of absorbed PAR (APAR) and absorbed NIR (ANIR). The modifications to MVP include: (1) tracking of multiple scattering within the canopy; (2) a mixed species canopy structure that consists of the dominant conifer layer at the top and the subdominant hardwood layer below with different canopy structure. Table 1 lists the canopy structural parameters for the pine and hardwood layers for 2001.

[9] MVP recognizes two types of gaps in the canopy: the between- and within-crown gaps. The between-crown gap probability is estimated based on geometric optics [*Li and Strahler*, 1985] as

$$P(n = 0|\theta_z) = e^{-\lambda_D A_T}, \tag{1}$$

where $P(.)$ is the between-crown gap probability; n is the number of tree crowns passed through by a sunbeam at a given solar zenith angle θ_z, λ_D is the stem density, and A_T is the shadowed area of an average tree crown on the ground. The within-crown gap probability is defined as the likelihood of a ray of direct radiation passing through at least one crown without being scattered (Figure 2). Assuming leaves are uniformly distributed within a crown, the within-crown gap probability can be computed as

$$P(n > 0|\theta_z) = e^{-\tau S_r} \tag{2}$$

where $\tau = K_b(\theta_z)F_v$ and has units of m^{-1}, $K_b(\theta_z)$ is the leaf area projection factor in the direction θ_z, F_v is the foliage area volume density (m^2 foliage area per m^3 crown volume), and S_r is the average path length that a sunbeam travels through tree crowns. For a gappy canopy, the path length of a sunbeam through the tree crowns is shorter than the path length through the canopy (S_a), i.e., $S_r < S_a$ as seen in Figure 2. For a single tree crown, the average path length for a sunbeam is $S_1 = V/[A_T \times \cos(\theta_z)]$, where V is the crown volume, and $A_T \times \cos(\theta_z)$ is the shadowed area projected perpendicular to the sunbeam. A sunbeam can pass through multiple crow e number of which depends on the solar zenith angle for a given stand [*Li and Wang*, 1995; *Song and Band*, 2004].

[10] Assuming independence of the gaps for the hardwood and conifer layers, the total between-crown gap probability for the entire canopy is

$$P_T(n = 0|\theta_z) = P_h(n = 0|\theta_z) \times P_c(n = 0|\theta_z), \tag{3}$$

where $P_T(n = 0|\theta_z)$, $P_h(n = 0|\theta_z)$, and $P_c(n = 0|\theta_z)$ are the total between-crown gap probability of the canopy, the between-crown gap probability for hardwood layer, and the between-crown gap probability for the conifer layer respectively. The total within-crown gap probability for the canopy is the convolution of the gap probabilities between the hardwood layer and the conifer layer, excluding total between-crown gap probability as

$$P_T(n > 0|\theta_z) = P_h(n|\theta_z) \otimes P_c(n|\theta_z) - P_T(n = 0|\theta_z), \tag{4}$$

where $\otimes$ indicates convolution. Details of probabilistic convolution can be found in the work of *Drake* [1967]. $P_T(n > 0|\theta_z)$ is the total within-crown gap probability of the canopy, and $P_h(n|\theta_z)$, and $P_c(n|\theta_z)$ are the probability for a beam of light at zenith angle θ_z passing n (n = 0, 1, 2, ...) crowns before reaching the forest floor.

[11] Diffuse light enters the canopy from all directions in the upper hemisphere. To estimate the amount of diffuse light traveling through the canopy, the gaps are integrated in all directions in the upper hemisphere for both the between- and within-crown gaps, i.e.

$$K_{open0} = \int_0^{\frac{\pi}{2}} P_T(n = 0|\theta_z)\sin(2\theta_z)d\theta_z, \tag{5}$$

and

$$K_{open1} = \int_0^{\frac{\pi}{2}} P_T(n > 0|\theta_z)\sin(2\theta_z)d\theta_z, \tag{6}$$

where K_{open0} and K_{open1} are called the openness factors for diffuse light traveling through the between- and within-crown gaps, respectively. Details of the model calculations for multiple scattering for GCR are given in Appendix B.

3.2. Modeling Latent Heat Flux

[12] Latent heat (LE) was modeled using the Penman-Monteith equation [*Monteith*, 1965]. The model is applied to sunlit and shaded leaves separately per unit LAI. The

Table 1. Structural Parameters for Conifer and Hardwood Layers in 2001 for the Loblolly Pine Stand Where the Flux Tower is Located

Parameter	Symbol	Conifer	Hardwoods
Lower canopy height (m)	h_1	9.4	2.6
Upper canopy height (m)	h_2	17.1	6.2
Stem density (trees/m^2)	λ_D	0.1377	0.147
Mean crown horizontal radius (m)	R	1.14	1.8
Crown shape	R_{br}	2.39	1.0

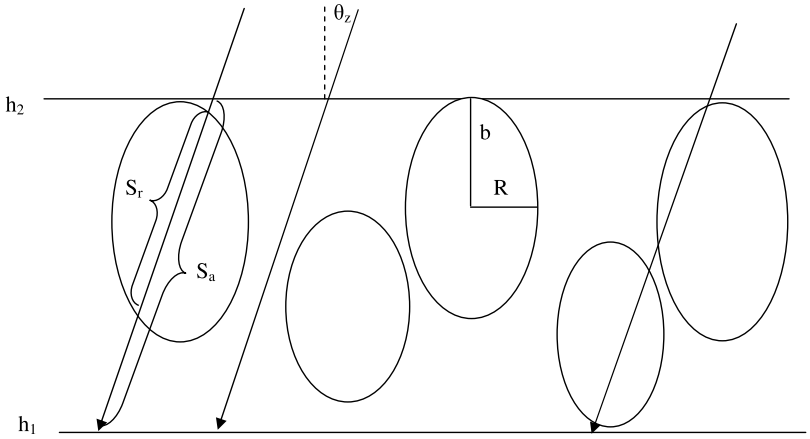

Figure 2. A single layer gappy canopy structure characterized by the upper canopy height (h_2), the lower canopy height (h_1), stem density, mean crown horizontal diameter (R), crown shape (b/R ratio), and leaf area index. There are two types of gaps in the canopy: the between- and within-crown gaps. For a gappy canopy, the path length of a sunbeam bypassing the canopy (S_a) is longer than the path length through the crowns (S_r). The sunbeam at zenith angle θ can pass no crowns, or one or more crowns, before reaching the forest floor. Modified from *Song and Band* [2004] with permission from NRC Research Press.

total canopy transpiration is the sum of the transpiration from all leaves. The model formulation, reviewed by *Eagleson* [2002], is given as:

$$LE_T = \frac{\Delta R_n + g_a \rho c_p [e_s(T) - e(T)]}{\Delta + \gamma_0 \left(1 + \frac{g_a}{g_{sw}}\right)}, \tag{7}$$

where LE_T is the latent heat flux due to transpiration per unit LAI, R_n is the net radiation per unit LAI; Δ is the slope of the saturated vapor pressure–temperature curve; γ is the surface psychrometric constant; ρ and c_p are the mean air density and specific heat capacity of dry air at constant pressure, respectively, and $e_s(T)$ and $e(T)$ are the saturated and actual vapor pressure at air temperature T, respectively. R_n, is estimated as

$$R_{\mathrm{n}} = \mathrm{APAR} + \mathrm{ANIR} + L_{\mathrm{c}}, \tag{8}$$

where APAR and ANIR are absorbed PAR and NIR, and L_c is the net long wave radiation of the canopy computed as the difference between outgoing long wave radiation emitted from the canopy and incoming long wave radiation from the atmosphere incident at the top and from forest floor at the bottom (see Appendix C for details). In equation (7), stomatal conductance for water g_{sw} was derived from stomatal conductance for carbon g_{sc} (g_{sw} = 1.56 × g_{sc}), which in turn was characterized by the Ball-Woodrow-Berry (referred to as BWB here after) stomatal conductance model [*Ball et al.*, 1987]. The aerodynamic conductance (g_a) was computed based on neutrally stratified rough-wall boundary layer formulations, reviewed by *Eagleson* [2002], as:

$$g_a = \left[\frac{\ln^2\left(\frac{h_2 - d_0}{z_0}\right)}{k_v^2 u_2}\right]^{-1}, \tag{9}$$

where h_2 is the canopy height, and d_0 and z_0 are the zero plane displacement and surface roughness, respectively. The wind speed at h_2 is u_2, and k_v is von Karman's constant (k_v = 0.4). Detailed closure models that can account for vertical variations of mean wind speeds inside the canopy are available (see *Katul et al.* [2004] for a review) though a separate sensitivity analysis (not shown here) suggested that the gains in model predictive skills were minor when accounting for the vertical variation of u. A model for forest floor evaporation is given in Appendix D. We did not include the evaporation from canopy interception in the model as the eddy-covariance instruments often do not capture this portion of vapor fluxes because the instruments cease to function properly when both instruments and the canopy are wet.

3.3. Modeling Photosynthesis

[13] Leaf photosynthesis was modeled by combining Fick's law, the BWB stomatal conductance model, and the photosynthesis model of *Farquhar et al.* [1980]:

$$A_n = g_{sc}(C_a - C_i), \tag{10}$$

$$g_{sc} = g_0 + m\frac{A_n H_r}{C_s}, \tag{11}$$

$$A_n = \min\left\{\begin{matrix} A_v \\ A_j \end{matrix}\right\} - R_d, \tag{12}$$

where A_n is the net photosynthesis of leaves, which yields the canopy-scale photosynthesis when integrated across the entire LAI. The canopy scale photosynthesis is equivalent to the Gross Ecosystem Production (GEP), which can be estimated based on ECMs as: GEP = NEE − RE, where NEE is net ecosystem exchange of CO_2 with the atmosphere

Table 2. Penman-Monteith and Farquhar Model Parameters[a]

Parameter	Definition	Unit	Value	Source
α	initial quantum yield		0.08	*Lai et al.* [2000]
a	PS II PAR absorbance		0.85	*Campbell and Norman* [1998]
C_a	ambient CO_2 concentration	ppm	370	this study
g_0	cuticular stomatal conductance	mol/m^2/s	0.015	*Lai et al.* [2000]
m	slope of g_c with respect to A_n		5.9	*Lai et al.* [2000]
K_{C25}	carboxylation at 25°C	pa	40.4	*De Pury and Farquhar* [1997]
K_{O25}	oxygenation at 25°C	pa	24.8×10^3	*De Pury and Farquhar* [1997]
$V_{0cmax25}$	carboxylation capacity	umol/m^2/s	72.5	*Lai et al.* [2002]
Q_{10Rub}	Q_{10} for Rubisco activity		2.4	*Thornton* [2000]
Q_{10C}	Q_{10} for carboxylation		2.1	*Thornton* [2000]
Q_{10O}	Q_{10} for oxygenation		1.2	*Thornton* [2000]
Θ_F	shape coefficient of the nonrectangular hyperbola		0.7	*De Pury and Farquhar* [1997]
$\omega(par/nir)$	leaf single scattering albedo		0.15/0.85	this study
k_n	nitrogen extinction coefficient		0.52	*Lai et al.* [2002]
D_s	soil depth	m	0.325	this study
p_o	porosity at soil surface		0.54	*Tague and Band* [2004]
p_d	porosity decay coefficient	1/m	4000.0	*Tague and Band* [2004]
K_{sat}	saturated conductance at surface	m/d	0.6	*Tague and Band* [2004]
k_d	K_{sat} decay coefficient with depth		0.24	*Tague and Band* [2004]
p_{si}	soil pore size index		0.186	*Tague and Band* [2004]
φ_e	air entry pressure	meters of water	0.478	*Tague and Band* [2004]

[a]For simulating evapotranspiration (ET) and photosynthesis, respectively, with both the uniform canopy representation (UCR) and gappy canopy representation (GCR).

directly measured at the flux tower, while RE, ecosystem respiration, needs to be estimated for daytime periods based on nighttime NEE data [*Stoy et al.*, 2006]. The rates A_v and A_j are the carboxylation-limited rate of net photosynthesis and the ribulose-biphosphate (RuBP) regeneration-limited rate of net photosynthesis. The CO_2 concentrations in the atmosphere, at the leaf surface, and in the leaf intercellular space are C_a, C_s and C_i, respectively. The mean relative humidity is H_r. We assume leaf surface boundary layer conductance is sufficiently large such that $C_s = C_a$. With these approximations, equations (10)–(12) can be solved for A_n, g_{sc} and C_i. The net photosynthesis is computed for sunlit and shaded leaves separately (see Appendix E for details).

3.4. Model Evaluations and Sensitivity Analyses

[14] A commonly used approach in identifying model parameters is through model calibration, which can lead to different parameters values for the same parameters in GCR and UCR. Adoption of different parameter values in UCR and GCR will obscure the effect of canopy structure on model results. Therefore, we used a set of identical model parameters published in the literature for both UCR and GCR models as listed in Table 2 and no model calibration was conducted. We should note that in Table 2, most of the physiological parameters were independently determined from gas exchange measurements [see *Lai et al.*, 2000]. As a result, the differences in the model results can be solely attributed to the difference in canopy structure. The impacts of canopy representation were evaluated first by comparing the modeling results between the two models, and then by comparing with corresponding entities from ECMs. We excluded the nighttime data from the flux tower for model evaluation because (1) canopy structure primarily influences radiation interception during daytime, and (2) eddy-covariance measurements at nighttime are less reliable.

[15] The loblolly pine stand where the flux tower resides is a closed canopy stan between-crown gap fractions are relatively small regardless which direction- solar radiation comes from. Differences between the two canopy representations are expected to be smallest for a closed canopy and increase as percent canopy cover declines. Testing the differences between the two models at this site highlights possibility for error due to a simple canopy representation even in the closed canopy condition. To generalize results, however, we also consider differences in model estimates across a range of canopy cover. A series of sensitivity analyses were performed to further quantify the impacts of canopy structure on the fluxes based on prescribed canopy structures. The sensitivity analysis provided more insights to the impacts of canopy structure on forest ecosystem processes. The sensitivity analysis we employed was based on a hypothetical single layer loblolly pine canopy with an average horizontal crown radius of 2.5 m, and canopy cover set at 0.2, 0.4, 0.6, and 0.8. Assuming random distribution of tree spatial locations in a stand, we estimated the stem density for canopy covers based on equation (1) with the sun at the zenith. The foliage area volume density was set at 0.7 m^2/m^3, leads to LAI of 1.25, 2.85, 5.11 and 9.00 for canopy cover at 0.2, 0.4, 0.6, and 0.8, respectively. Due to crown overlap, LAI increases more than canopy cover in relative proportions. The upper and lower canopy heights were derived using the allometric relationships for loblolly pine based on the crown diameter, which was determined with data collected in the stands around the study site [*Song*, 2007]. The canopy structural parameters for the sensitivity analysis are given in Table 3. The meteorological variables measured at the flux tower for 2001 were used as model inputs.

4. Results

4.1. Net Radiation

[16] Modeled daytime half-hourly R_n by UCR and GCR for the loblolly pine stand are highly correlated ($R^2 = 0.97$), but R_n from UCR is about 8% lower than that from GCR

Table 3. Canopy Structural Parameters for the Sensitivity Analysis[a]

Parameters	Symbols	Canopy Cover 0.2	0.4	0.6	0.8
Lower canopy height (m)	h_1	12.8	12.8	12.8	12.8
Upper canopy height (m)	h_2	21.2	21.2	21.2	21.2
Stem density (trees/m^2)	λ_D	0.0114	0.0260	0.0467	0.0820
Mean crown horizontal radius (m)	R	2.5	2.5	2.5	2.5
Leaf area index	LAI	1.25	2.85	5.11	9.00
Crown shape	R_{br}	2.39	2.39	2.39	2.39

[a]The crown horizontal radius and canopy cover are prescribed first, and then h_1 and h_2 are derived based on allometry for loblolly pine collected in the field [*Song*, 2007]. The stem density is derived based on the assumption that the crowns are randomly distributed in space, and the LAI is derived based on the assumption that the foliage volume density is 0.7 m^2/m^3.

(Figure 3a). Intuitively we would expect that a uniform canopy should intercept more radiation than a gappy canopy. We further examined radiation interception in the canopy and on the forest floor. In fact, UCR intercepted nearly 17% more shortwave solar radiation in the canopy than did GCR (Figure 3b), but the forest floor under UCR received less than 60% of shortwave radiation than that under GCR for the loblolly pine stand (Figure 3c). Because leaves are highly reflective to NIR, a uniform canopy reflects more NIR than a gappy canopy does. In addition, UCR reduces NIR reaching the forest floor where most of it will be absorbed. The shortwave radiation received on the forest floor under GCR more than compensated for the lower shortwave radiation interception in the forest canopy. This is why UCR produced lower R_n for the stand than GCR. Thus, the two types of canopy structure differ more in the distribution of radiation than the total radiation absorbed by the stand. *Yang et al.* [2001] reached similar conclusions with a 3D vegetation canopy in a soil-vegetation-atmosphere-transfer model in the old jack pine stand of the southern study site of the Boreas project [*Sellers et al.*, 1997].

[17] Given the results in Figure 3, a question remains as to whether R_n was underestimated by UCR or overestimated by GCR. We searched for the answer by comparing the modeled results with measurements. Figure 4 clearly indicates that GCR provided a more accurate estimate of measured R_n than UCR. GCR reduced the root mean squared error (RMSE) by nearly 50% compared with UCR. The modeled R_n from UCR is almost 11% lower than the measured R_n (R^2 = 0.93, RMSE = 63.3 W/m^2), while the modeled R_n from GCR is within 3% of the measured R_n (R^2 = 0.97, RMSE = 33.6 W/m^2). It is important to note that even for this closed canopy loblolly pine stand with relatively high leaf area index (Figure 1), canopy structure still matters in modeling R_n for the stand.

4.2. Latent Heat Exchange

[18] LE modeled by UCR and GCR are also highly correlated (R^2 = 0.98). Although UCR produced R_n approximately 8% lower that that from GCR, the latent heat flux produced by UCR is about 8% higher than that from GCR (Figure 5a). This is because UCR intercepted nearly 17% more shortwave radiation than GCR (Figure 3b), indicating that about half of the additional energy intercepted in UCR is used for transpiration. We took the difference between each pair of points in Figure 5a and plotted the difference against time of day (Figure 5b). The difference between the two models is strongly related to solar angle, reaching a maximum around noon. At high solar elevation angle, the between-crown gaps in GCR are largest, allowing more radiation to pass through the canopy and reach the forest floor. Thus UCR produced higher LE than GCR.

[19] Due to the high correlation between the model results, LE from both models correlates similarly and strongly with the measured LE from the flux tower (Figures 6a and 6b), but the slope between GCR and measured LE is almost unity. It is obvious that the comparison between the modeled and the measured quantities is not as good for LE as for R_n. Three major factors may have contributed to the scatter in Figure 6 observed between the modeled and measured LE: (1) scale mismatch between the model and the flux tower measure-

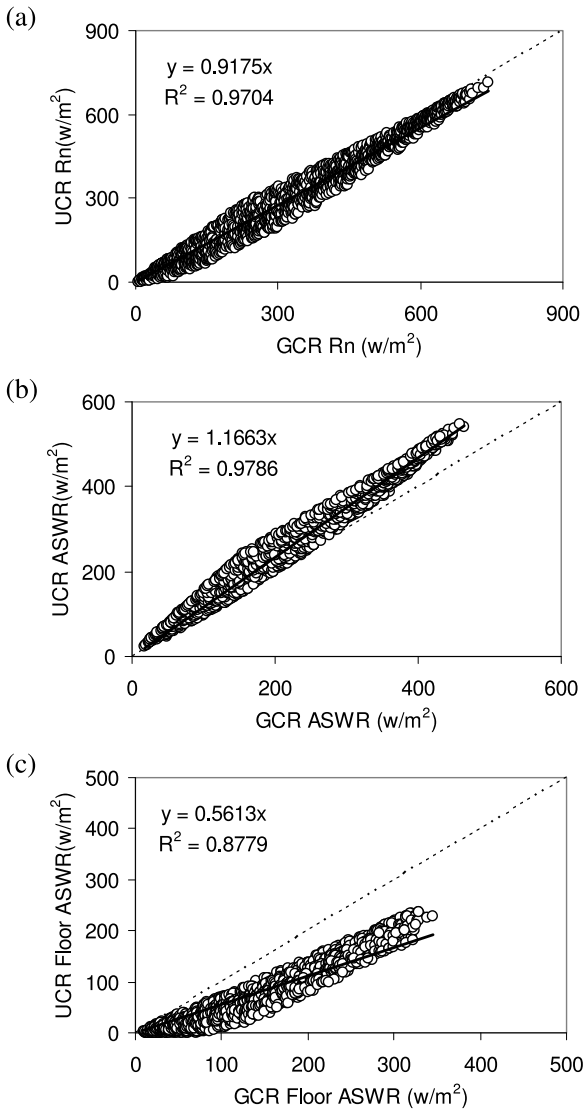

Figure 3. Comparison of modeled radiation for the loblolly pine stand between UCR and GCR: (a) net radiation (R_n) for the stand; (b) absorbed shortwave radiation (ASWR) in the canopy; (c) ASWR on the forest floor.

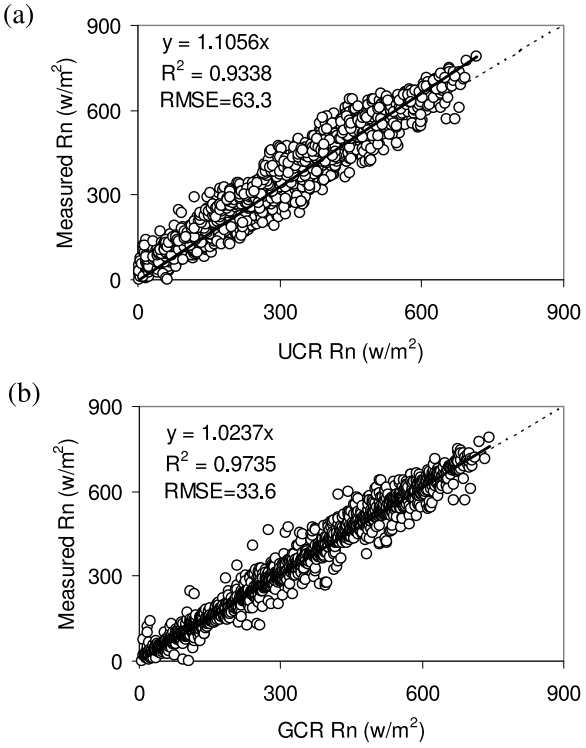

Figure 4. Comparison of modeled half-hourly R_n with the measured R_n on the flux tower: (a) UCR; (b) GCR.

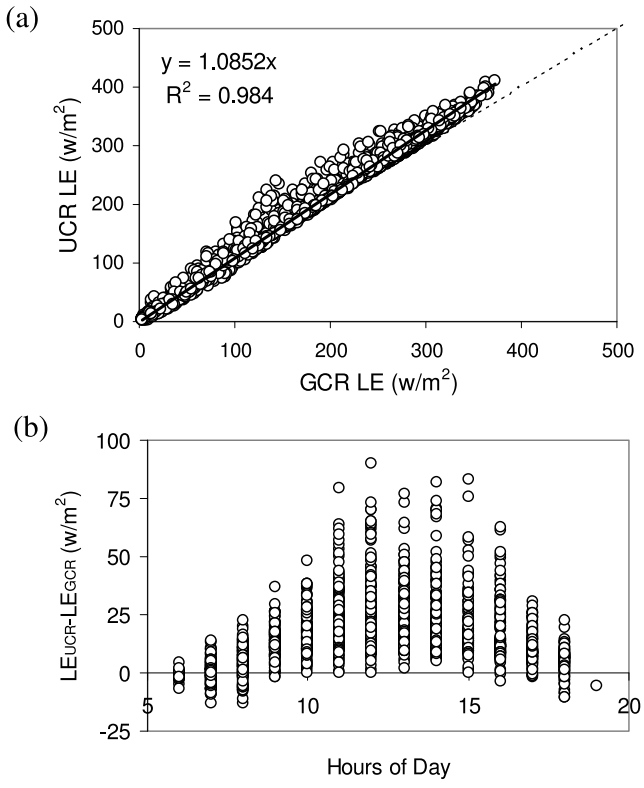

Figure 5. Comparison of modeled half-hourly LE between UCR and GCR: (a) Modeled LE; (b) difference in modeled LE. LE from UCR is about 8.5% higher than that from GCR. Most of the difference between the two models occurs around noon when the gaps in GCR are best seen from the direction of th ent sunbeam.

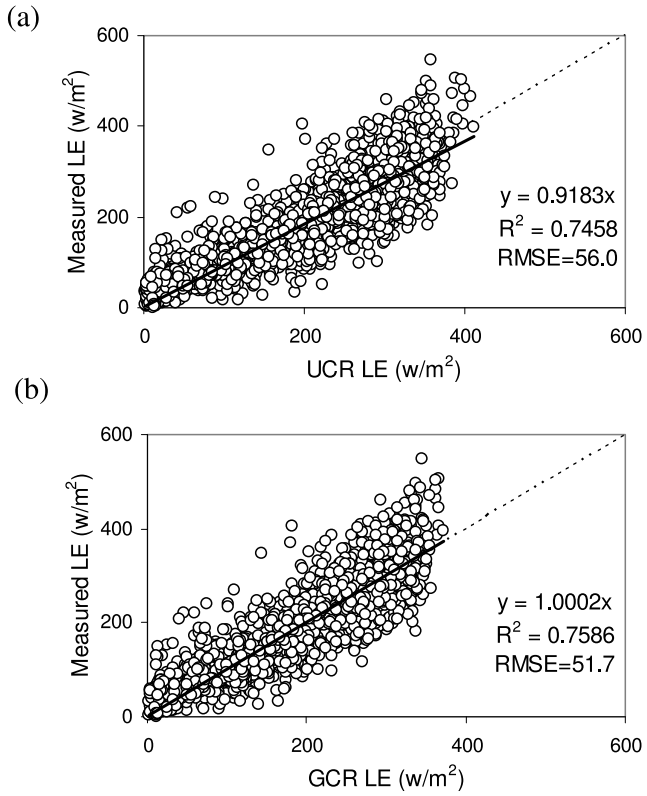

Figure 6. Comparison of modeled LE with measured LE on the flux tower at half-hourly time step: (a) UCR; (b) GCR.

ments, (2) random variation from flux tower measurements due to the dynamic nature of the flux footprint [*Oren et al.*, 2006], and (3) errors in model parameters in Penman-Monteith equation. If we consider the daytime trend for the entire growing season, LE from GCR better matches with the measured LE than that from UCR (Figure 7). When comparing the ensemble mean diurnal trends, we essentially removed the high frequency random errors from the eddy

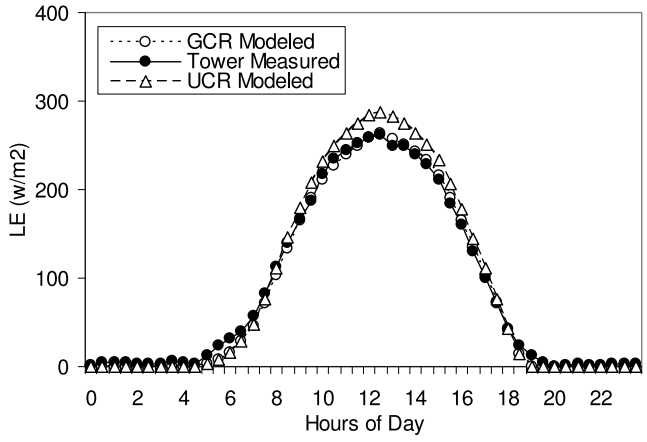

Figure 7. Comparison of modeled LE with measured LE on the flux tower for the daytime trend for the growing season of 2001.

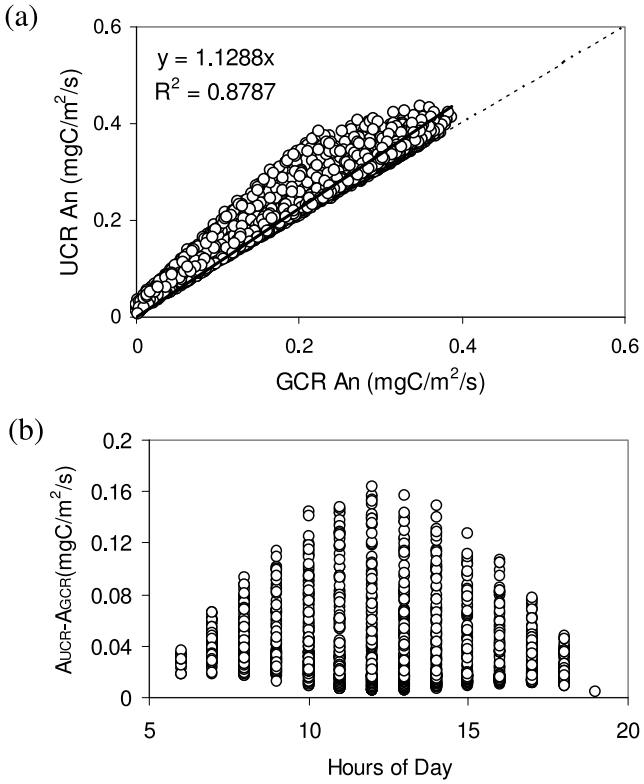

Figure 8. Comparison of modeled half-hourly A_n between UCR and GCR: (a) Modeled A_n; (b) difference in modeled A_n.

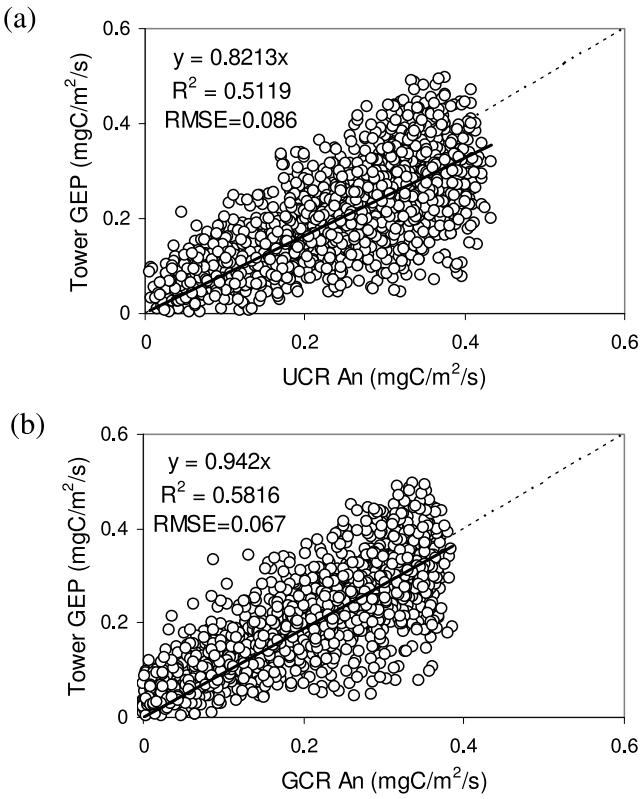

Figure 9. Comparison of modeled half-hourly A_n from UCR and GCR with GEP from ECMs: (a) UCR; (b) GCR. A_n from GCR has a higher R^2 and significantly smaller RMSE than that from UCR.

flux measurements, which could account for 50% of the variation at the half hourly time step [*Oren et al.*, 2006].

4.3. Net Photosynthesis

[20] A_n between UCR and GCR (Figure 8a) are less well correlated compared with LE (Figure 5a). A_n from UCR is about 13% higher than that from GCR. Though highly correlated, there is a nonlinear component between A_n from UCR and GCR as UCR asymptotes with respect to GCR. Again, the difference between the estimates progressively increases and maximizes at the time when the sun reached its highest point, and then decreases (Figure 8b). When compared with GEP derived from the flux tower measurements (Figures 9a and 9b), the relationship is much poorer than that for LE. Although the R^2 between model and measurements is slightly higher for GCR, it is fairly low for both models. The slopes in Figures 9a and 9b are both less than unity, indicating modeled A_n is higher than tower GEP. However, the slope of the relationship between GCR and the tower GEP is much closer to unity than that for UCR. Therefore, A_n from UCR has a much larger positive bias than that from GCR. Several factors may influence data scattering in Figures 9a and 9b. First, the size of modeled stand and the footprint of the flux tower may not match, which will reduce the strength of the relationship similar to latent heat. Second, GEP is not directly measured by the eddy-covariance system; rather it is derived using a flux partitioning model for NEE. It is inevitable that additional uncertainties can be introduced during the process [*Stoy et al.*, 2006], further reducin the correlation of modeled A_n and GEP. Third, ECMs contain error on the order of 12% for daytime carbon flux [*Anthoni et al.*, 1999]. Nevertheless, significant improvement of GCR over UCR can be seen when comparing the daytime trend between modeled A_n and GEP derived from tower measurements (Figure 10).

4.4. Sensitivity Analysis of Canopy Structure

[21] The difference between the modeled A_n by UCR and GCR for stands with canopy cover ranging from 0.2 to 0.8 is

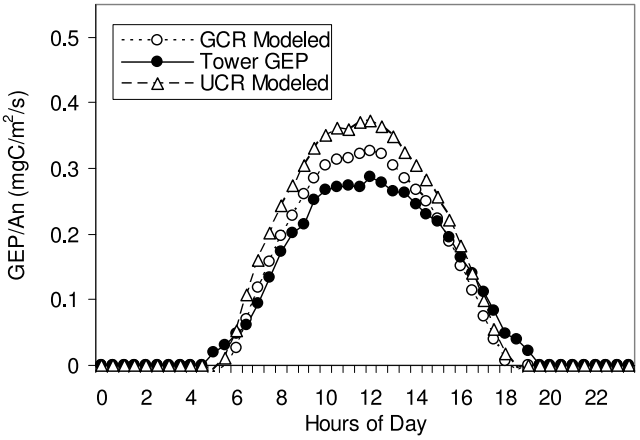

Figure 10. Comparison of daytime trend of A_n from UCR and GCR with GEP from ECMs during the growing season of 2001.

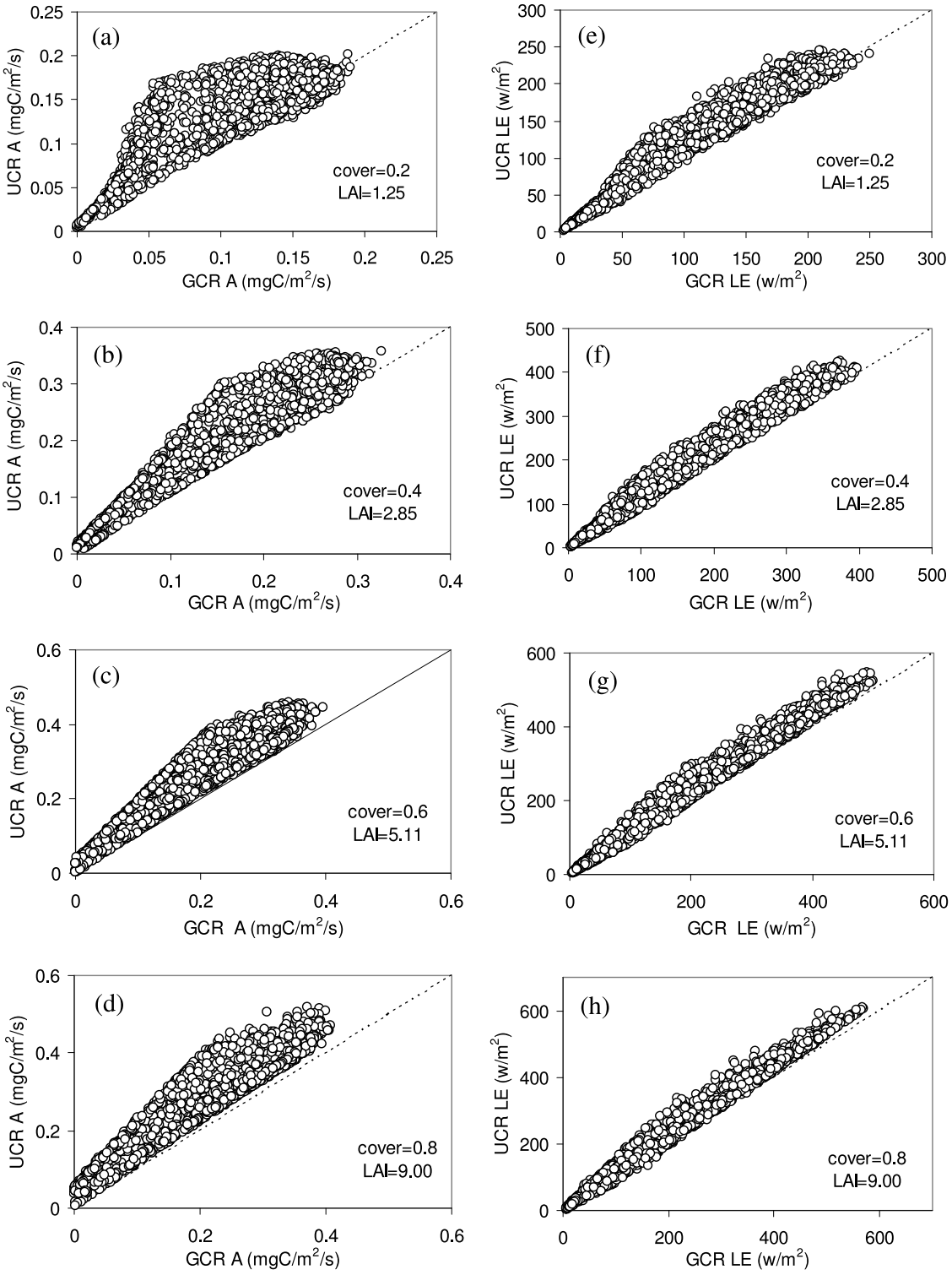

Figure 11. Sensitivity analysis for A_n: (a) cover is 0.2, LAI is 1.25; (b) cover is 0.4, LAI is 2.85; (c) cover is 0.6, LAI is 5.11; (d) cover is 0.8, LAI is 9.00; and LE: (e) cover is 0.2, LAI is 1.25; (f) cover is 0.4, LAI is 2.85; (g) cover is 0.6, LAI is 5.11; (h) cover is 0.8, LAI is 9.00.

shown in Figures 11a–11d. Because photosynthesis responds nonlinearly to radiation absorption, there is not a simple one-to-one relationship between the two canopy representations under identical environmental conditions for the same stands. There is a very high degree of nonlinearity between deled by the two approaches when the canopy cover is low. The nonlinearity dampens as the canopy cover increases, but A_n from UCR is consistently higher than that of GCR, even with canopy cover at 0.8. A_n from UCR reaches an asymptote with respect to that from GCR. The differences in A_n between the two models for the loblolly pine stand closely resemble that seen here at high

canopy cover. The difference increases as A_n increases. High A_n occurs during the peak growing season at the time when the sun angle is high [*Schäfer et al.*, 2003]. This is the time when the largest portion of gaps (in the GCR representation) in stands can be seen in the direction of the sunbeam, allowing more sunlight to reach the forest floor. This is also the time when radiation interception by UCR differs most from that by GCR.

[22] Similarly, LE from UCR is also higher than that from GCR for all canopy covers (Figures 11e–11h). The relative differences are larger when canopy cover is lower. The latent heat fluxes modeled with the two canopy representations are more linearly related compared with net photosynthesis, and the relationship strengthens as the canopy cover increases. The strong linear relationship at higher canopy cover for the latent heat flux between the two canopy representations indicates that the differences can be calibrated by adjusting the empirical parameters in the model, such as the slope parameter in the BWB model in equation (11). However, such calibration only produces phenomenological agreement between the modeled and measured LE. It contributes little to our understanding of the processes.

[23] Figure 12 shows the differences obtained through the sensitivity analysis between GCR and UCR at the stand scale (i.e., combining the canopy component with the corresponding component on the forest floor) for APAR, ANIR, effective long wave radiation and the net radiation of canopies with coverage at 0.4 (Figures 12a–12d) and 0.8 (Figures 12e–12h). It is clear that UCR absorbed more PAR and much less NIR than GCR. Regardless of canopy cover, there is nearly no difference between the two canopy structures in the effective long wave radiation under the current modeling condition. Detailed examination of all radiation components of canopy and the forest floor separately at each canopy coverage (not shown) indicates that UCR absorbed much more PAR in the canopy than GCR. The relative difference is larger at low canopy cover, but the absolute difference in the amount of PAR absorbed by UCR is larger when the canopy cover is high. A similar trend is seen for NIR in the canopy, but the differences are much smaller. On the forest floor, the opposite trend is seen. GCR absorbed much more NIR on the forest floor than UCR, and the relative differences increases with canopy cover, although the absolute differences decrease with canopy cover due to strong canopy reflectance. Combining the energy balance in the forest canopy and on the forest floor, the total net radiation for the stand is higher for GCR than that for UCR, and the differences increases with canopy cover within the range of cover analyzed. This modeling result also indicates that the gappy canopy created by thin and tall tree crowns as boreal forests more effectively at absorbing radiation than a uniform canopy.

5. Discussion

[24] Proper representation of canopy structure is a key element in ecosystem models. LAI was the most important component of the canopy under the traditional "big-leaf" up-scaling scheme [*Monteith*, 1965; *Sinclair et al.*, 1976; *Running and Hunt*, 1993]. However, the nonlinear response of leaf carbon assimila light interception can create appreciable bias when scaling up canopy carbon assimilation using the big-leaf approach. To avoid the bias with the big-leaf scaling up scheme, multilayer models were developed where the plant canopy was divided into a number of parallel horizontal layers [*Duncan et al.*, 1967; *Baldocchi*, 1993; *Raupach and Finnigan*, 1988]. More recent multilayer models consider the transfer of momentum, heat, water vapor, and CO_2 between the biosphere and the atmosphere and resolve all the way-way interactions between leaves and their immediate microclimate using higher order turbulent transport theories [*Juang et al.*, 2008]. These models solve for all the sources and sinks, fluxes, leaf and air temperature, leaf internal variables, and mean concentration profiles within the canopy volume. Canopy assimilation and transpiration were estimated as the sum of those from all layers. Multilayer canopy representation in ecosystem models can provide improved estimates of carbon assimilation and transpiration in the canopy. However, the computational need for ecosystem models with multilayer representation of vegetation canopies and the challenge to provide model parameters for each layer make such models practically impossible for operational use over a heterogeneous landscape. Although it is possible in principle to test multilayer models with field data, this is difficult in practice [*Amthor*, 1994].

[25] A middle ground between the big-leaf and the multilayer canopy model was established later on, i.e., replacing the big-leaf model with two-leaf model for a single layer canopy. Instead of separating the canopy into multiple layers, leaves in a single layer were separated into sunlit and shaded leaves to account for the nonlinearity in ecosystem processes to light intensity, and the single layer two-leaf model compared very well with multilayer models [*De Pury and Farquhar*, 1997; *Wang and Leuning*, 1998]. The two-leaf model assumes a random distribution of leaves in the canopy space. This study takes the two-leaf model one step closer to reality by accounting for between-crown gaps. A two-leaf single layer model with between-crown gaps can significantly improve the model performance in modeling energy, water and carbon fluxes. Although the two-leaf model accounting between crown gaps is computationally efficient, it requires five more detailed canopy structural parameters (Table 1). These structural parameters are difficult to obtain, particularly over large areas. However, we may not need to estimate all five parameters independently as crown radius is related to canopy height through allometry, and crown radius and stem density are constrained by canopy cover. Moreover, recent advances in remote sensing both with high spatial resolution optical sensors to extract LAI and tree crown size [*Song and Dickinson*, 2008; *Song*, 2007; *Clark et al.*, 2004; *Leckie et al.*, 2003] and with Lidar to extract canopy height [*Lefsky et al.*, 2002; *Sun et al.*, 2008] are making it possible to extract these canopy structural parameters as input to GCR.

[26] This study investigated the impacts of two contrasting canopy representations, a uniform canopy representation (UCR) and a gappy canopy representation (GCR), on modeling ecosystem energy, water and carbon fluxes in a loblolly pine stand in Duke Forest, near Durham, North Carolina. Both UCR and GCR modeled the total R_n very well as supported by the good agreement with the measurements. However, they differ greatly in the partitioning of solar

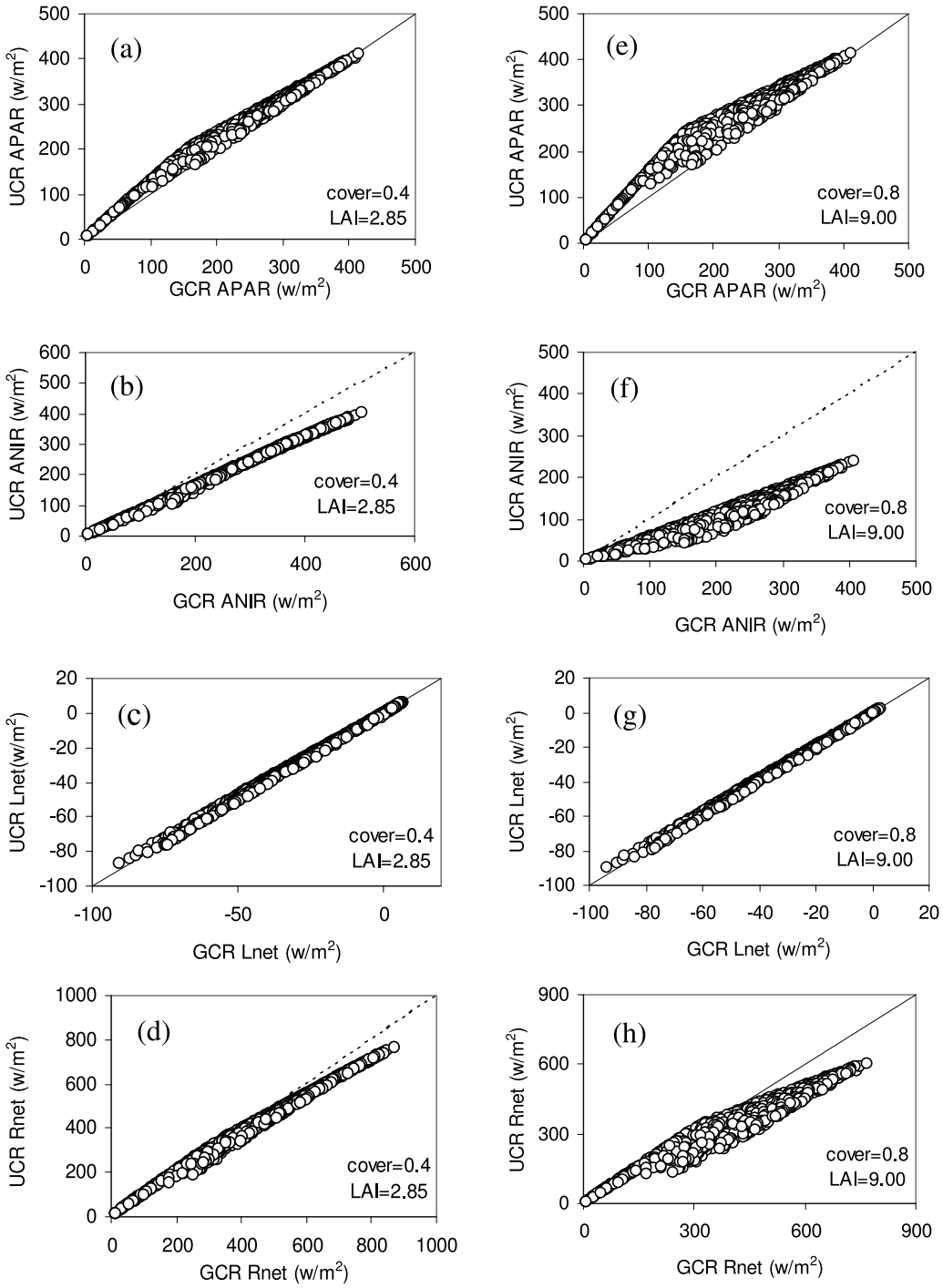

Figure 12. Sensitivity analysis for APAR, ANIR, effective long wave radiation, and net radiation for canopy cover at 0.4: (a) APAR, (b) ANIR, (c) effective long wave radiation, and (d) net radiation; and cover at 0.8: (e) APAR, (f) ANIR, (g) effective long wave radiation, and (h) net radiation.

radiation intercepted in the canopy versus the forest floor. More radiation on the forest floor may have large effects on other ecological processes, such as regeneration, including the establishment and growth of seedlings [*Tognetti et al.*, 1997; *McGuire et al.*, 2001; *Naumburg et al.*, 2001], or heat flow into the soil, which influences other ecosystem processes, such as decomposition and forest floor CO_2 efflux [*Palmroth et al.*, 2005; *Daly et al.*, 2009]. Because carbon assimilation is a canop ess, the difference in radiation interception in the canopy is reflected in the estimates of A_n (Figure 7a), but a smaller difference was seen in LE, a process occurring in both the canopy and forest floor (Figure 5a). Overestimation of radiation interception in the canopy with UCR can lead to overestimation of carbon assimilation using remotely sensed data based on light use efficiency [*Running et al.*, 1994; *Landsberg and Waring*, 1997]. Therefore, the uniform canopy assumption for the canopy structure may not be acceptable when the goal is to

estimate energy use in the canopy or forest floor regardless of forest cover. Due to the high correlation for LE between UCR and GCR, it may be argued that UCR can be used for successful phenomenological modeling of latent heat transfer with proper calibration. However, the uniform canopy assumption poses a problem for modeling carbon assimilation even for the closed canopy loblolly pine stand. Thus, large errors may be generated when uniform canopy structure models are used to estimate carbon assimilation over grid size of several kilometers or larger because a large grid tends to include nonforest more likely. These errors cannot be calibrated by adjusting linear scalar empirical parameters in the models due to the nonlinearity in the process [*Medlyn et al.*, 2005].

[27] This study found that accounting for canopy structure is a significant step forward in modeling vegetated surface radiation balance, and subsequent energy-driven ecosystem processes. Stand scale canopy structure is generally missing or significantly simplified in the current biosphere models at continental or global scale applications [*Sellers et al.*, 1996; *Foley et al.*, 1996; *Haxeltine and Prentice*, 1996; *Woodward et al.*, 1998]. Given the availability of remote sensing from Lidar sensors, it is possible to incorporate canopy structure into these models for local or regional scale applications. *Huang et al.* [2008] attempted to incorporate the three-dimensional canopy structure into the CASA model [*Potter et al.*, 1993] to evaluate the impacts of selective logging on carbon cycling. *Hilker et al.* [2008] successfully used Lidar data to capture canopy gaps in scaling up GEP derived from flux tower. Effective incorporation of vegetation canopy structure into ecosystem process models for regional or large area applications is becoming more feasible with recent advances in remote sensing, and what is now missing is the efficient incorporation of such measurements with processes known to nonlinearly scale with leaf area and other structural attributes.

6. Conclusions

[28] Canopy structure has a significant impact on the distribution of energy between the canopy and forest floor. For the loblolly pine stand in the Duke Forest studies here, UCR intercepted nearly 17% more shortwave radiation in the canopy, and over 40% less shortwave radiation on the forest floor compared with GCR during the growing season of 2001. Combining the canopy and the forest floor, GCR provided much more accurate estimation of R_n for the stand than UCR. Based on the model results, UCR estimated higher A_n and LE than GCR. Limited improvement is seen for GCR over UCR for A_n and LE when comparing the data from the flux tower at the half hourly time step, but becomes clearer when comparing the daytime trend over the growing season with ECM. A sensitivity analysis found that A_n and LE from UCR are higher than those from GCR across a range of canopy cover from 0.2 to 0.8. The relationship between the net photosynthesis from the two models is highly nonlinear at low canopy cover. The nonlinearity decreases as the canopy cover increases, but never disappears. The relationship for LE from GCR and UCR are much stronger compared with A_n, and the strength of the linear relationship increases as canopy cover increases. Given the availability of advanced technologies, such as Lidar and high resolution optical images that provide spatially explicit information of canopy structures of vegetation, it is now possible to investigate the impacts of canopy structure on ecosystem functions over a heterogeneous landscape using models with GCR provided this heterogeneity is not too severe to impact processes outside the light and radiation environment.

Appendix A: Radiation Transfer Through Uniform Canopies

[29] Modeling radiation transport through uniform canopies (i.e., UCR) is based on *Campbell and Norman* [1998]. Radiation in the photosynthetically active spectrum (PAR) and near-infrared spectrum (NIR) are modeled separately. Total absorbed radiation within the canopy is the sum of the absorbed PAR and NIR from sunlit and shaded leaves. We assume a spherical leaf angle distribution in the canopy. The extinction coefficient for beam light is

$$K_b(\theta_z) = \frac{\sqrt{x^2 + \tan^2(\theta_z)}}{x + 1.774(x + 1.182)^{-0.733}} \tag{A1}$$

where θ_z is solar zenith angle. For spherical leaf angle distribution, $x = 1$. The transmittance of beam radiation is

$$\tau_b(\theta_z) = \exp(-K_b(\theta_z)L), \tag{A2}$$

where L is leaf area index. The transmittance of beam radiation with scattering in the canopy is

$$\tau_{bt}(\theta_z) = \exp\left(-K_b(\theta_z)\sqrt{\alpha}L\right), \tag{A3}$$

where α is absorptance. Similarly, the transmittance of diffuse light is

$$\tau_{dt} = \exp\left(-K_d\sqrt{\alpha}L\right), \tag{A4}$$

where K_d is the extinction coefficient of diffuse radiation, and

$$K_d = -\ln(\tau_d)/L, \tag{A5}$$

where

$$\tau_d = \int_0^{\pi/2} \tau_b(\theta)\sin(2\theta)d\theta \tag{A6}$$

[30] Therefore, the total unintercepted beam plus down scattering beam, $I_{bt}(\theta_z)$, the unintercepted beam only, $I_b(\theta_z)$, and the diffuse flux, J, under the forest canopy are, respectively

$$I_{bt}(\theta_z) = \tau_{bt}(\theta_z) \times {}^0I, \tag{A7}$$

$$I_b(\theta_z) = \tau_b(\theta_z) \times {}^0I, \tag{A8}$$

and

$$J = \tau_{dt} \times {}^0J \tag{A9}$$

where ${}^0I$ and ${}^0J$ are the direct and diffuse radiation at the top of canopy, respectively. The flux density of scattering beam radiation at the bottom of the canopy is

$$I_{sc} = I_{bt}(\theta_z) - I_b(\theta_z) \tag{A10}$$

[31] Because the scattering beam radiation flux density is zero at the top of canopy, the average beam scattering radiation flux density ($\overline{I}_{sc}$) for the entire canopy can be considered as

$$\overline{I}_{sc} = I_{sc}/2 \tag{A11}$$

[32] The beam radiation on sunlit leaves is a constant regardless where the leaves are in the canopy. However, the diffuse radiation is J^0 at the top of the canopy, and J at the bottom of the canopy. Thus the exponentially averaged diffuse radiation should be used as the mean flux density of diffuse radiation on the leaves as

$$\overline{J} = {}^0J \frac{[1 - \exp(-\sqrt{\alpha}K_d L)]}{\sqrt{\alpha}K_d L}. \tag{A12}$$

[33] Therefore, the mean flux density on the sunlit leaves is

$$I_{sunlit}(\theta_z) = K_b(\theta_z){}^0I + \overline{J} + \overline{I}_{sc}, \tag{A13}$$

and the mean flux density on the shaded leaves is

$$I_{shaded} = \overline{J} + \overline{I}_{sc}. \tag{A14}$$

[34] The sunlit LAI in a canopy is

$$L_{sunlit} = \frac{1 - \exp(-K_b(\theta_z)L)}{K_b(\theta_z)}. \tag{A15}$$

[35] Separating sunlit and shaded leaves in modeling canopy transpiration and carbon assimilation requires that the input solar radiation in two components, direct (${}^0I$) and diffuse (${}^0J$). However, the flux tower only provides a total PAR measurement. We estimated PAR is 41% of shortwave radiation based on data measured on the tower in 2004 and 2005. Separation of total radiation into direct and diffuse components is based on *Liu and Jordan* [1960] and *Leuning* [1995]. The amount of diffuse radiation is a function of atmospheric transmissivity (τ_a). Since the total radiation is available from the tower, the total τ_a can be estimated as

$$\tau_a = \frac{Q}{S_0\left(1 + 0.033\cos\left(2\pi\left(J_{day} - 10\right)/365\right)\right)\sin(h)}, \tag{A16}$$

where S_0 is the solar constant (1367.0 W/m^2). J_{day} is the Julian date, and h is solar elevation angle. Q is the measured total solar radiation, i.e. ${}^0I + {}^0J$. The number 365 is the number of days in a year, and J_{day} takes the value within [1,365]. The fraction of diffuse radiation is estimated as

$$f_d = \begin{cases} 1 & \tau_a < 0.3 \\ 1 - 2(\tau_a - 0.3) & 0.3 \le \tau_a \le 0.7 \\ 0.2 & \tau_a > 0.7 \end{cases}, \tag{A17}$$

where f_d is the fraction of diffuse radiation. Therefore, ${}^0J = f_d \times Q$, and ${}^0I = Q - {}^0J$.

Appendix B: Radiation Transport Through Gappy Canopies

[36] Radiation propagation through gappy canopies (i.e., GCR) is based on *Song and Band* [2004], but we modified the algorithm to account for mixed species as described in equations (3)–(6) with more rigorous treatment of multiple scattering as NIR radiation is added in this study. Radiation in the PAR and NIR spectra are simulated separately, and the total absorbed radiation is the sum of absorbed PAR and NIR from sunlit and shaded leaves respectively. At the first collision with the leaves, the amount of direct radiation absorbed by the canopy is

$${}^1I = [(1.0 - P_T(n = 0|\theta_z) - P_T(n > 0|\theta_z)] \times {}^0I \times (1.0 - \omega), \tag{B1}$$

where $P_T(n = 0|\theta_z)$ is the total between-crown gap probability including both coniferous and hardwood species, and n is the number of crowns that a beam passing through the canopy, and θ_z is the solar zenith angle. $P_T(n > 0|\theta_z)$ is the within-crown gap probability including coniferous and hardwood species. The leaf single scattering albedo is ω. The amount of diffuse radiation absorbed by the canopy is

$${}^1J = \left[\left(1.0 - K_{open0} - K_{open1}\right] \times {}^0J \times (1.0 - \omega), \tag{B2}$$

where K_{open0} and K_{open1} are openness factors as described in equations (5) and (6). Subsequent multiple scattering between the canopy and the background is traced through successive orders of scattering. Our numerical experiments found that five orders of successive tracing are accurate enough (higher order tracing leads to change < 0.1 W/m^2). The single scattering source at the forest floor includes direct and diffuse radiation passing through gaps in the canopy, and the scattered radiation by the leaves when photons first hit the leaves. The amount of direct radiation passing through the canopy without collision with leaves is

$${}^0I^{\downarrow} = [P_T(n = 0|\theta_z) + P_T(n > 0|\theta_z)] \times {}^0I, \tag{B3}$$

and the amount of diffuse PAR reaching the forest floor without scattering is

$${}^0I^{\downarrow} = \left[K_{open0} + K_{open1}\right] \times {}^0J. \tag{B4}$$

[37] Assuming half of the direct and diffuse radiation scattered by the leaves go downward when photons first hit

the leaves, the amount of direct radiation scattered downward from the canopy is:

$$^1I = [1.0 - P_T(n = 0|\theta_z) - P_T(n > 0|\theta_z)] \times {}^0I \times \omega/2.0, \quad \text{(B5)}$$

and the amount of diffuse radiation scattered downward from the canopy is

$$^1J = \left[\left(1.0 - K_{\text{open0}} - K_{\text{open1}}\right] \times {}^0J \times \omega/2.0. \quad \text{(B6)}$$

[38] Therefore, the first order scattering source at the forest floor is

$$^1S = {}^0I^{\downarrow} + {}^1I + {}^0J + {}^1J \quad \text{(B7)}$$

[39] The reflected radiation from the forest floor at first scattering is $\rho_s \times {}^1S$, where ρ_s is the background albedo. Assuming the reflected radiation from the forest floor is uniformly distributed in all upper hemispherical directions, some of the reflected radiation will exit through the canopy gaps. Some of the radiation will be absorbed again by the canopy, and can be modeled by

$$^2J = \rho_s \times {}^1S \times \left[1.0 - K_{\text{open0}} - K_{\text{open1}}\right] \times (1.0 - \omega). \quad \text{(B8)}$$

[40] Assuming half of the second order scattered photon go downward, then the second order scattering source radiation at the forest floor is

$$^2S = \rho_s \times {}^1S \times \left[\left(1.0 - K_{\text{open0}} - K_{\text{open1}}\right] \times \omega/2. \quad \text{(B9)}$$

[41] The second order scattering from the forest floor will be reabsorbed in the canopy, and some of it will be reflected back to be the source of third order scattering. This multiple scattering process continues in the model until a preset threshold (0.1 W/m^2 here) is met such that subsequent multiple scattering is considered negligible. The total radiation absorbed for sunlit leaves includes the absorbed direct radiation at the first collision with leaves and subsequent absorption of scattered direct and diffuse radiation. The total absorbed radiation for shaded leaves include absorption of scattered direct and diffuse radiation. Similar to equation (A15), the sunlit leaf area index is estimated as

$$L_{\text{sunlit}} = \frac{1.0 - P_T(n = 0|\theta_z) - P(n > 0|\theta_z)}{K_b(\theta_z)}, \quad \text{(B10)}$$

where $K_b(\theta_z)$ is calculated by equation (A1).

Appendix C: Modeling Long Wave Radiation

[42] R_n is modeled for sunlit and shaded leaves, and forest floor, respectively. The total R_n for the stand is the sum of R_n from these three components. The total absorbed shortwave radiation for sunlit and shaded leaves is the sum of absorbed PAR and NIR, which is described in Appendix A (the uniform canopy) and Appendix B (the gappy canopy). R_n is the total absorbed shortwave radiation from the sun minus the long wave effective radiation. Leaves in the canopy absorb long wave radiation from the atmosphere and the forest floor. Leaves likewise emit long wave radiation such that

$$L_{\text{nc}} = \left(1.0 - K_{open0} - K_{open1}\right)\left(L_a - 2L_c + L_f\right), \quad \text{(C1)}$$

where L_{nc} is the canopy net long wave radiation, L_a is the downward long wave radiation from the atmosphere, L_c is the long wave radiation from the forest canopy, and L_f is the long wave radiation from the forest floor. K_{open0} and K_{open1} are the openness factors for between- and within-crown gaps as defined in equations (5) and (6). For UCR, there is only K_{open1}. We assume the forest canopy absorbs all the long wave radiation except that which passes through the gaps. The forest canopy emits long wave radiation toward both the atmosphere and forest floor, requiring the factor of two in equation (C1). The emission of long wave radiation is modeled as

$$L_i = \varepsilon_i \sigma T_i^4, \quad \text{(C2)}$$

where the subscript i refers to a, c and f for atmosphere, canopy and the floor, respectively. T_a (K) is the atmospheric temperature which is used for L_a and L_c, soil temperature is used for L_f. The atmospheric emissivity (ε_a) is modeled based on *Unsworth and Monteith* [1975] as

$$\varepsilon_a = (1 - 0.84c)\varepsilon_{a0} + 0.84c, \quad \text{(C3)}$$

where c is the cloud cover and ε_{a0} is the clear sky emissivity, which is modeled after *Brutsaert* [1975] as

$$\varepsilon_{a0} = 1.24\left(\frac{e_a}{T_a}\right)^{\frac{1}{7}}, \quad \text{(C4)}$$

where e_a is the vapor pressure in millibars, and T_a is in degrees Kelvin. Emissivity for the canopy (ε_c) and forest floor (ε_f) are set as 0.98 and 0.95, respectively [*Chen et al.*, 2005]. Cloud cover in equation (C3) was inferred indirectly from the solar radiation measured on the flux tower. We first estimated the actual transmittance with clouds as

$$\tau_c = \frac{R_{sw}}{S_0\left(1.0 + 0.033\cos\left(2\pi\left(J_{day} - 10.0\right)/365.0\right)\right)\cos(\theta_z)}, \quad \text{(C5)}$$

[43] Where R_{sw} is the measured total shortwave radiation on a horizontal surface at the flux tower, and S_0 is solar constant (1367 w/m^2). J_{day} is Julian date, and θ_z is solar zenith angle. Assuming atmospheric transmittance for a cloudless sky is 0.7, cloud cover in equation (C3) is estimated as

$$c = 1.0 - \tau_c/0.7, \quad \text{(C6)}$$

[44] Net long wave radiation on the forest floor (L_{nf}) is estimated as

$$L_{\mathrm{nf}} = \left(K_{open0} + K_{open1}\right)L_a + \left(1.0 - K_{open0} - K_{open1}\right)L_c - L_f \tag{C7}$$

Appendix D: Modeling Forest Floor Evaporation

[45] Evaporation from the forest floor is computed using equation (7) by replacing the stomatal conductance with soil conductance, which is simulated following *Tague and Band* [2004] as

$$g_{\mathrm{sl}} = \begin{cases} 0.001429 & \theta_{\mathrm{v}} > 0.185 \\ 1/(-83000\theta_{\mathrm{v}} + 16100) & \text{otherwise} \end{cases}, \tag{D1}$$

where g_{sl} is the soil conductance to water for evaporation, and θ_v is the soil volumetric water content. Soil surface evaporation is limited either by availability of energy for evaporation or by the potential soil surface exfiltration, given by

$$\mathrm{LE_E} = \min\{\mathrm{LE_v}, \mathrm{LE_x}\}, \tag{D2}$$

where LE_E is the latent heat flux due to evaporation at the forest floor and LE_v is the potential latent heat flux from evaporation based on equation (7) where the stomatal conductance is replaced with soil conductance; R_n on the forest floor is used. For simplicity, we used g_a in the canopy instead of modeling g_a for the forest floor separately as forest floor evaporation is a minor component of LE [*Oren et al.*, 1998]. LE_x is the potential latent heat flux limited by soil exfiltration modeled as

$$LE_x = S^{\frac{1}{2p_{si}}+2}\sqrt{\frac{8\overline{p}_o\overline{K}_{sat}\varphi_e}{3(1+3p_{si})(1+4p_{si})}}, \tag{D3}$$

where S is the relative soil water saturation, which takes value within [0,1] and φ_e is the air entry pressure. The soil pore size index is p_{si}, and the average soil porosity is $\overline{p}_o$. Assuming porosity decreases with soil depth exponentially, the average soil porosity can be estimated as

$$\overline{p}_o = p_d \times p_0[1 - \exp(-D_s/p_d)], \tag{D4}$$

where p_d is the pore size decay coefficient with soil depth, and p_0 is the soil porosity at the surface, where the soil depth is D_s. Similarly, the average saturated soil conductance for water, $\overline{K}_{sat}$, in equation (12) is calculated as

$$\overline{K}_{sat} = k_d \times K_{sat}[1 - \exp(-D_s/k_d)], \tag{D5}$$

where K_{sat} is the saturated conductance of water at the soil surface, and k_d is the decay coefficient of K_{sat} with soil depth.

Appendix E: Modeling Photosynthesis

[46] Implementation of the Farquhar photosynthesis model [*Farquhar et a* 0] follows *Thornton* [2000]. The carboxylation-limited and RuBP regeneration-limited net photosynthesis rate are, respectively,

$$A_{\mathrm{v}} = \frac{V_{\mathrm{cmax}}\left(C_i - \Gamma^*\right)}{C_{\mathrm{i}} + \mathrm{K_C}\left(1 + \mathrm{O}/\mathrm{K_O}\right)} - R_{\mathrm{d}} \tag{E1}$$

and

$$A_{\mathrm{j}} = \frac{J\left(C_{\mathrm{i}} - \Gamma^*\right)}{4.5C_{\mathrm{i}} + 10.5\Gamma^*} - R_{\mathrm{d}}, \tag{E2}$$

where C_i is the leaf space CO_2 concentration, and O is the leaf space oxygen concentration. V_{cmax} is the maximum rate of carboxylation, which depends on leaf nitrogen content. Nitrogen content in the canopy is assumed decrease exponentially with depth. Thus, the total carboxylation capacity in the canopy is

$$V_{cc\max 25} = L^* V_{0c\max 25}(1.0 - \exp(-k_n L))/k_n \tag{E3}$$

[47] $V_{0cmax25}$ is the maximum carboxylation rate at 25°C at the top of the canopy. $V_{0cmax25}$ is derived from *Lai et al.* [2002] where V_{cmax} at the top of canopy at 28°C was measured as 84.5 umol/m^2/s for the same stand, and k_n is the nitrogen extinction coefficient which was also taken from *Lai et al.* [2002]. $V_{ccmax25}$ is total canopy carboxylation capacity at 25°C, which will be dynamically distributed between sunlit and shaded leaves. V_{cmax25} for sunlit leaf at 25°C is set as $V_{0cmax25}$, and the remaining carboxylation capacity is distributed among the shaded leaves. The total canopy carboxylation capacity is held constant at a given LAI. The effect of temperature on the carboxylation rate is modeled as

$$V_{c\max} = \frac{\mathrm{V_{cmax25}}\exp(a_1(T-25))}{1 + \exp(a_2(T-41))} \tag{E4}$$

where a_1 and a_2 are empirical parameters, and are set as 0.051 and 0.205 based on measurements [*Lai et al.*, 2000]. In this study, we assume that aerodynamic conductance is sufficiently large so that we can use air temperature for leaf temperature. K_C in equation (D1) is the carboxylase reaction constant, which is modeled as

$$K_{\mathrm{C}} = \begin{cases} K_{C25} \times (Q_{10Kc})^{\frac{T-25}{10}} & T > 15^\circ C \\ K_{C25} \times (1.8 \times Q_{10Kc})^{\frac{T-15}{10}}/Q_{10Kc} & T < 15^\circ C \end{cases}, \tag{E5}$$

where K_{C25} is K_C at the temperature of 25°C, and Q_{10Kc} is the rate of increase in K_C with an increase of 10°C in temperature. K_O in equation (19) is the oxygenase reaction constant modeled as

$$K_{\mathrm{O}} = K_{O25} \times (Q_{10Ko})^{\frac{T-25}{10}}, \tag{E6}$$

where K_{O25} is the K_O at the reference temperature (25°C). Q_{10Ko} is the rate of increase of K_O with an increase of 10°C in temperature, and Γ* in equations (E1) and (E2) is CO_2

concentration for photosynthesis compensation in the absence of dark respiration (R_d). It can be modeled using

$$\Gamma^* = \frac{0.5V_{o\max}K_C O}{V_{c\max}K_O}, \tag{E7}$$

where $V_{o\max}$ is the maximum oxygenation rate of Rubisco. Following Biome-BGC [*Thornton*, 2000], we assumed $V_{o\max}/V_{c\max}$ = 0.21. J in equation (E2) is the potential electron transport rate, and is solved from the following according to *De Pury and Farquhar* [1997]

$$\Theta_F J^2 - (a\alpha_J I + J_{\max})J + a\alpha_J I J_{\max} = 0, \tag{E8}$$

where $J_{\max}$ is the maximum rate of electron transport per leaf area, and $J_{\max}$ = $2.1V_{c\max}$. [*Wullschleger*, 1993; *De Pury and Farquhar*, 1997]. The electron transport quantum use efficiency (α_J) is derived from the quantum yield for photosynthesis as [*Medlyn et al.*, 2000]:

$$\alpha = \frac{a_J(C_i - \Gamma^*)}{4C_i + 2\Gamma^*}, \tag{E9}$$

[48] The dark respiration, R_d in equations (E1) and (E2), is modeled following *Collatz et al.* [1991] using

$$R_d = 0.015V_{c\max}, \tag{E10}$$

[49] To solve equations (E1) and (E2), we require the leaf space CO_2 concentration, C_i, which is solved by inverting Fick's law, $A = g_{sc}(C_a - C_i)$. Due to the nonlinear response of photosynthesis to photon flux density, the Farquhar photosynthesis model was applied to sunlit and shaded leaves separately [*De Pury and Farquhar*, 1997], and the total assimilation rate is the weighted average of the assimilation rates for the sunlit and shaded leaves, i.e.

$$A = A_{\text{sunlit}}\ \text{LAI}_{\text{sunlit}} + A_{\text{shaded}}\ \text{LAI}_{\text{shaded}} \tag{E11}$$

where A is the net photosynthesis rate for the canopy (μmol $CO_2/m^2/s$). A_{sunlit} and A_{shaded} are total net photosynthesis rate for sunlit and shaded leaves, respectively.

[50] **Acknowledgments.** The support for Conghe Song on the research is provided by NSF grant 035143 and NASA grant NNX06AE28G. Conghe Song thanks John M. Norman at the University of Wisconsin-Madison for his help with understanding the uniform canopy model used in this paper. The fieldwork for measurements of canopy structure in the area was partly supported by USDA Forest Service Agenda 2020 program. EC measurements were supported by the Office of Science (BER), U.S. Department of Energy, through its Southeast Regional Center (SERC) of the National Institute for Global Environmental Change (NIGEC) under cooperative agreements DE-FC03-90ER61010 and DE-FC02-03ER63613, through BER's FACE FACTS-I project, grant DE-FG02-95ER62083, and the National Science Foundation (NSF-EAR-0628342 and NSF-EAR 0635787).

References

Amthor, J. S. (1994), Scaling CO_2-photosynthesis relationships from the leaf to the canopy, *Photosynth. Res.*, *39*, 321–350, doi:10.1007/BF00014590.

Anthoni, P. M., B. E. Law, and M. H. Unsworth (1999), Carbon and water vapor exchange of an open-canopied ponderosa pine ecosystem, *Agric. For. Meteorol.*, *95*(3), 151–168 doi:10.1016/S0168-1923(99)00029-5.

Baldocchi, D. D. (1993), Scaling water vapor and carbon dioxide exchange from leaves to a canopy: Rules and tools, in *Scaling Physiological Processes: Leaf to Globe*, edited by J. R. Ehleringer and C. B. Field, pp. 77–114, Academic, San Diego, Calif.

Baldocchi, D., et al. (2001), FLUXNET: A new tool to study the temporal and spatial variability of ecosystem-scale carbon dioxide, water vapor, and energy flux densities, *Bull. Am. Meteorol. Soc.*, *82*(11), 2415–2434, doi:10.1175/1520-0477(2001)082<2415:FANTTS>2.3.CO;2.

Ball, J. T., I. E. Woodrow, and J. A. Berry (1987), A model predicting stomatal conductance and its contribution to the control of photosynthesis under different environmental conditions, in *Progress in Photosynthesis Research*, vol. 4, edited by J. Beggens, Martinus Nijhoff, Dordrecht, Netherlands.

Betts, R. A., P. M. Cox, and S. E. Lee (1997), Contrasting physiological and structural vegetation feedbacks in climate change simulations, *Nature*, *387*(6635), 796–799, doi:10.1038/42924.

Betts, R. A., et al. (2007), Projected increase in continental runoff due to plant responses to increasing carbon dioxide, *Nature*, *448*(7157), 1037–1041, doi:10.1038/nature06045.

Brutsaert, W. (1975), On a derivable formula for long-wave radiation from clear skies, *Water Resour. Res.*, *11*(5), 742–744, doi:10.1029/WR011i005p00742.

Campbell, G. S., and J. M. Norman (1998), *An Introduction to Environmental Biophysics*, 2nd ed., Springer, New York.

Chen, J. M., and S. G. Leblanc (1997), A four-scale bidirectional reflectance model based on canopy architecture, *IEEE Trans. Geosci. Remote Sens.*, *35*(5), 1316–1337, doi:10.1109/36.628798.

Chen, J. M., et al. (2000), Recent advances in geometrical optical modelling and its applications, *Remote Sens. Rev.*, *18*(2–4), 227–262.

Chen, J. M., et al. (2005), Distributed hydrological model for mapping evapotranspiration using remote sensing inputs, *J. Hydrol. Amsterdam*, *305*, 15–39, doi:10.1016/j.jhydrol.2004.08.029.

Clark, D. B., et al. (2004), Application of 1-m and 4-m resolution satellite data to ecological studies of tropical rain forests, *Ecol. Appl.*, *14*, 61–74, doi:10.1890/02-5120.

Collatz, G. J., et al. (1991), Physiological and environmental-regulation of stomatal conductance, photosynthesis and transpiration—A model that includes a laminar boundary-layer, *Agric. For. Meteorol.*, *54*, 107–136, doi:10.1016/0168-1923(91)90002-8.

Daly, E., et al. (2009), The effects of elevated atmospheric CO_2 and nitrogen amendments on subsurface CO_2 production and concentration dynamics in a maturing pine forest, *Biogeochemistry*, *94*(3), 271–287, doi:10.1007/s10533-009-9327-7.

De Pury, D. G. G., and G. D. Farquhar (1997), Simple scaling of photosynthesis from leaves to canopies without the errors of big-leaf models, *Plant Cell Environ.*, *20*, 537–557, doi:10.1111/j.1365-3040.1997.00094.x.

Detto, M., et al. (2006), Soil moisture and vegetation controls on evapotranspiration in a heterogeneous Mediterranean ecosystem on Sardinia, Italy, *Water Resour. Res.*, *42*, W08419, doi:10.1029/2005WR004693.

Drake, A. W. (1967), *Fundamental of Applied Probability Theory*, McGraw-Hill, New York.

Duncan, W. G., et al. (1967), A model for simulating photosynthesis in plant communities, *Hilgardia*, *38*(4), 181–205.

Eagleson, P. S. (2002), *Ecohydrology: Darwinian Expression of Vegetation Form and Function*, Cambridge Univ. Press, Cambridge, U. K.

Ewers, B. E., and R. Oren (2000), Analysis of assumptions and errors in the calculation of stomatal conductance from sap flux measurements, *Tree Physiol.*, *20*, 579–590.

Farquhar, G. D., S. von Caemmerer, and J. A. Berry (1980), A biochemical model of photosynthetic CO_2 assimilation in leaves of C_3 species, *Planta*, *149*, 78–90, doi:10.1007/BF00386231.

Foley, J. A., et al. (1996), An integrated biosphere model of land surface processes, terrestrial carbon balance, and vegetation dynamics, *Global Biogeochem. Cycles*, *10*, 603–628, doi:10.1029/96GB02692.

Friend, A. D., et al. (1997), A process-based, terrestrial biosphere model of ecosystem dynamics (Hybrid v3.0), *Ecol. Modell.*, *95*, 249–287, doi:10.1016/S0304-3800(96)00034-8.

Gedney, N., P. M. Cox, and R. A. Betts (2006), Detection of a direct carbon dioxide effect in continental river runoff records, *Nature*, *439*(7078), 835–838, doi:10.1038/nature04504.

Goel, N. S. (1988), Models of vegetation canopy reflectance and their use in estimation of biophysical parameters from reflectance data, *Remote Sens. Rev.*, *4*, 1–212.

Haxeltine, A., and I. C. Prentice (1996), BIOME3: An equilibrium terrestrial biosphere model based on ecophysiological constraints, resource availability, and competition among plant functional types, *Global Biogeochem. Cycles*, *10*, 693–709, doi:10.1029/96GB02344.

Hilker, T., et al. (2008), A modeling approach for upscaling gross ecosystem production to the landscape scale using remote sensing data, *J. Geophys. Res.*, *113*, G03006, doi:10.1029/2007JG000666.

Hsieh, C. I., G. Katul, and T. Chi (2000), An approximate analytical model for footprint estimation of scalar fluxes in thermally stratified atmospheric flows, *Adv. Water Resour.*, *23*, 765–772, doi:10.1016/S0309-1708(99)00042-1.

Huang, M., et al. (2008), An ecosystem model for tropical forest disturbance and selective logging, *J. Geophys. Res.*, *113*, G01002, doi:10.1029/2007JG000438.

Juang, J. Y., et al. (2008), Investigating a hierarchy of Eulerian closure models for scalar transfer inside forested canopies, *Boundary Layer Meteorol.*, *128*, 1–32, doi:10.1007/s10546-008-9273-2.

Katul, G. G., et al. (2004), One and two equation models for canopy turbulence, *Boundary Layer Meteorol.*, *113*, 81–109, doi:10.1023/B:BOUN.0000037333.48760.e5.

Kucharik, C. J., J. M. Norman, and S. T. Gower (1999), Characterization of radiation regimes in nonrandom forest canopies: Theory, measurements, and a simplified modeling approach, *Tree Physiol.*, *19*(11), 695–706.

Lai, C. T., et al. (2000), Modeling CO_2 and water vapor turbulent flux distributions within a forest canopy, *J. Geophys. Res.*, *105*, 26,333–26,351, doi:10.1029/2000JD900468.

Lai, C. T., et al. (2002), Modelling the limits on the response of net carbon exchange to fertilization in a south-eastern pine forest, *Plant Cell Environ.*, *25*, 1095–1119, doi:10.1046/j.1365-3040.2002.00896.x.

Landsberg, J. J., and R. H. Waring (1997), A generalized model of forest productivity using simplified concepts of radiation-use efficiency, carbon balance and partitioning, *For. Ecol. Manage.*, *95*, 209–228, doi:10.1016/S0378-1127(97)00026-1.

Leckie, D. G., et al. (2003), Stand delineation and composition estimation using semi-automated individual tree crown analysis, *Remote Sens. Environ.*, *85*, 355–369, doi:10.1016/S0034-4257(03)00013-0.

Lefsky, M. A., et al. (2002), Lidar remote sensing ofr ecosystem studies, *BioScience*, *52*(1), 19–30, doi:10.1641/0006-3568(2002)052[0019:LRSFES]2.0.CO;2.

Leuning, R. (1995), A critical-appraisal of a combined stomatal-photosynthesis model for C_3 plants, *Plant Cell Environ.*, *18*, 339–355, doi:10.1111/j.1365-3040.1995.tb00370.x.

Li, X., and A. H. Strahler (1985), Geometric-optical modeling of a conifer forest canopy, *IEEE Trans. Geosci. Remote Sens.*, *GE-23*, 705–721, doi:10.1109/TGRS.1985.289389.

Li, X., and J. Wang (1995), *Geometric Optical Models for Remote Sensing of Vegetation and Parameterization for Vegetation Structure*, Sci. Press, Beijing, China.

Li, X., A. H. Strahler, and C. E. Woodcock (1995), A hybrid geometric optical-radiative transfer approach for modeling albedo and directional reflectance of discontinuous canopies, *IEEE Trans. Geosci. Remote Sens.*, *33*, 466–480, doi:10.1109/36.377947.

Liu, B. Y. H., and R. C. Jordan (1960), The interrelationship and characteristic distribution of direct, diffuse and total solar radiation, *Sol. Energy*, *4*, 1–19, doi:10.1016/0038-092X(60)90062-1.

McCarthy, H. R., et al. (2007), Temporal dynamics and spatial variability in the enhancement of canopy leaf area under elevated atmospheric CO_2, *Global Change Biol.*, *13*(12), 2479–2497, doi:10.1111/j.1365-2486.2007.01455.x.

McGuire, J. P., et al. (2001), Gaps in a gappy forest: Plant resources, longleaf pine regeneration, and understory response to tree removal in longleaf pine savannas, *Can. J. For. Res.*, *31*(5), 765–778, doi:10.1139/cjfr-31-5-765.

Medlyn, B. E., et al. (2000), Soil processes dominate the long-term response of forest net primary productivity to increased temperature and atmospheric CO_2 concentration, *Can. J. For. Res.*, *30*, 873–888, doi:10.1139/cjfr-30-6-873.

Medlyn, B. E., et al. (2005), On the validation of models of forest CO_2 exchange using eddy covariance data: Some perils and pitfalls, *Tree Physiol.*, *25*, 839–857.

Monteith, J. L. (1965), Evaporation and the environment, in *Proceedings of the 19th Symposium of the Society for Experimental Biology*, pp. 205–233, Cambridge Univ. Press, New York.

Myneni, R. B., J. Ross, and G. Asrar (1989), A review on the theory of photon transport in leaf canopies, *Agric. For. Meteorol.*, *45*, 1–153, doi:10.1016/0168-1923(89)90002-6.

Naumburg, E., D. S. Ellsworth, and G. G. Katul (2001), Modeling dynamic understory photosynthesis of contrasting species in ambient and elevated carbon dioxide, *Oecologia*, *126*(4), 487–499, doi:10.1007/s004420000543.

Ni, W., et al. (1997), Transmission of solar radiation in boreal conifer forests: Measurements and models, *J. Geophys. Res.*, *102*(D24), 29,555–29,566, doi:10.1029/97JD00198.

Oren, R., et al. (1998), Water balance delineates the soil layer in which moisture affects canopy conductance, *Ecol. Appl.*, *8*, 990–1002, doi:10.1890/1051-0761(1998)008[0990:WBDTSL]2.0.CO;2.

Oren, R., et al. (2006), Estimating the uncertainty in annual net ecosystem carbon exchange: Spatial variation in turbulent fluxes and sampling errors in eddy-covariance measurements, *Global Change Biol.*, *12*, 883–896, doi:10.1111/j.1365-2486.2006.01131.x.

Palmroth, S., et al. (2005), Contrasting responses to drought of forest floor CO_2 efflux in a loblolly pine plantation and a nearby oak-hickory forest, *Global Change Biol.*, *11*, 421–434, doi:10.1111/j.1365-2486.2005.00915.x.

Potter, C. S., et al. (1993), Terrestrial ecosystem production - a process model-based on global satellite and surface data, *Global Biogeochem. Cycles*, *7*, 811–841, doi:10.1029/93GB02725.

Pukkala, T., et al. (1991), Predicting spatial-distribution of direct-radiation below forest canopies, *Agric. For. Meteorol.*, *55*(3–4), 295–307, doi:10.1016/0168-1923(91)90067-Z.

Raupach, M. R., and J. J. Finnigan (1988), Single-layer models of evaporation form plant canopies are incorrect but useful, whereas multilayer models are correct but useless: Discuss, *Aust. J. Plant Physiol.*, *15*, 705–716.

Running, S. W., and J. C. Coughlan (1988), A general model of forest ecosystem processes for regional applications: I. Hydrologic balance, canopy gas exchange and primary production processes, *Ecol. Modell.*, *42*, 125–154, doi:10.1016/0304-3800(88)90112-3.

Running, S. W., and E. R. Hunt (1993), Generalization of a forest ecosystem process model for other biomes, BIOME-BGC, and an application for global scale models, in *Scaling Physiological Processes: Leaf to Globe*, edited by J. R. Ehleringer and C. B. Field, pp. 141–158, Academic, San Diego, Calif.

Running, S. W., et al. (1994), Terrestrial remote sensing science and algorithms planned for EOS MODIS, *Int. J. Remote Sens.*, *15*(17), 3587–3620, doi:10.1080/01431169408954346.

Ryan, M. G. (2002), Canopy processes research, *Tree Physiol.*, *22*(15–16), 1035–1043.

Schäfer, K. V. R., et al. (2002), Hydrologic balance in an intact temperate forest ecosystem under ambient and elevated atmospheric CO_2 concentration, *Global Change Biol.*, *8*, 895–911, doi:10.1046/j.1365-2486.2002.00513.x.

Schäfer, K. V. R., et al. (2003), Exposure to an enriched CO_2 atmosphere alters carbon assimilation and allocation in a pine forest ecosystem, *Global Change Biol.*, *9*, 1378–1400, doi:10.1046/j.1365-2486.2003.00662.x.

Sellers, P. J., et al. (1996), A revised land surface parameterization (SiB2) for atmospheric GCMs. Part I: Model formulation, *J. Clim.*, *9*, 676–705, doi:10.1175/1520-0442(1996)009<0676:ARLSPF>2.0.CO;2.

Sellers, P. J., et al. (1997), BOREAS in 1997: Experiment overview, scientific results, and future directions, *J. Geophys. Res.*, *102*(D24), 28,731–28,769, doi:10.1029/97JD03300.

Sinclair, T. R., C. E. Murphy, and K. R. Knoerr (1976), Development and evaluation of simplified models for simulating canopy photosynthesis and transpiration, *J. Appl. Ecol.*, *13*, 813–829, doi:10.2307/2402257.

Song, C. (2007), Estimating tree crown size with spatial information of high resolution optical remotely sensed imagery, *Int. J. Remote Sens.*, *28*(15), 3305–3322, doi:10.1080/01431160600993413.

Song, C., and L. E. Band (2004), MVP: A model to simulate the spatial patterns of photosynthetically active radiation under discrete forest canopies, *Can. J. For. Res.*, *34*, 1192–1203, doi:10.1139/x03-280.

Song, C., and M. B. Dickinson (2008), Extracting forest canopy structure from spatial information of high resolution optical imagery: Tree crown size and leaf area index, *Int. J. Remote Sens.*, *29*(19), 5605–5622, doi:10.1080/01431160802060904.

Stoy, P. C., et al. (2006), An evaluation of models for partitioning eddy covariance-measured net ecosystem exchange into photosynthesis and respiration, *Agric. For. Meteorol.*, *141*(1), 2–18, doi:10.1016/j.agrformet.2006.09.001.

Suits, G. H. (1983), Extension of a uniform canopy reflectance model to include row effects, *Remote Sens. Environ.*, *13*, 113–129, doi:10.1016/0034-4257(83)90017-2.

Sun, G., et al. (2008), Forest vertical structure from GLAS: An evaluation using LVIS and SRTM data, *Remote Sens. Environ.*, *112*, 107–117, doi:10.1016/j.rse.2006.09.036.

Tague, C. L., and L. E. Band (2004), RHESSys: Regional Hydro-Ecologic Simulation System—An object-oriented approach to spatially distributed modeling of carbon, water and nutrient cycling, *Earth Interact.*, *8*, 1–42, doi:10.1175/1087-3562(2004)8<1:RRHSSO>2.0.CO;2.

Tang, Y. H., et al. (1999), Heterogeneity of light availability and its effects on simulated carbon gain of tree leaves in a small gap and the understory in a tropical rain forest, *Biotropica*, *31*(2), 268–278, doi:10.1111/j.1744-7429.1999.tb00138.x.

Thornton, P. E. (2000), Biome-BGC version 4.1.1, Numer. Terradyn. Simul. Group, Sch. of For., Univ. of Mont., Missoula.

Tognetti, R., J. D. Johnson, and M. Michelozzi (1997), Ecophysiological response of Gagus Sylvatica seedlings to changing light conditions. 1. Interactions between photosynthetic acclimation and photoinhibition during simulated canopy gap formation, *Physiol. Plant.*, *101*, 115–123, doi:10.1111/j.1399-3054.1997.tb01827.x.

Unsworth, M. H., and J. L. Monteith (1975), Long-wave radiation at the ground: I. Angular distribution of incoming radiation, *Q. J. R. Meteorol. Soc.*, *101*, 13–24.

Wang, Y. P., and P. G. Jarvis (1990), Description and validation of an array model–MAESTRO, *Agric. For. Meteorol.*, *51*, 257–280, doi:10.1016/0168-1923(90)90112-J.

Wang, Y. P., and R. Leuning (1998), A two-leaf model for canopy conductance, photosynthesis and partitioning of available energy I: Model description and comparison with a multi-layered model, *Agric. For. Meteorol.*, *91*, 89–111, doi:10.1016/S0168-1923(98)00061-6.

Woodward, F. I., M. R. Lomas, and R. A. Betts (1998), Vegetation-climate feedbacks in a greenhouse world, *Philos. Trans. R. Soc. London, Ser. B*, *353*, 29–38, doi:10.1098/rstb.1998.0188.

Wullschleger, S. D. (1993), Biochemical limitations to carbon assimilation in C_3 plants—A retrospective analysis of the A/C_i curves from 109 species, *J. Exp. Bot.*, *44*, 907–920, doi:10.1093/jxb/44.5.907.

Yang, R., M. A. Friedl, and W. G. Ni (2001), Parameterization of shortwave radiation fluxes for nonuniform vegetation canopies in land surface models, *J. Geophys. Res.*, *106*(D13), 14,275–14,286, doi:10.1029/2001JD900180.

L. E. Band and C. Song, Department of Geography, University of North Carolina at Chapel Hill, Chapel Hill, NC 27599, USA. (csong@email.unc.edu)

G. Katul and R. Oren, Nicholas School of Environment, Duke University, Durham, NC 27708, USA.

H. R. McCarthy, Department of Earth System Science, University of California, Irvine, CA 92697, USA.

P. C. Stoy, School of GeoSciences, University of Edinburgh, Edinburgh EH9 3JN, UK.

C. L. Tague, Donald Bren School of Environment and Management, University of California, Santa Barbara, CA 93106, USA.